

Fluxtube Dynamics in Neutron Star Cores

Vanessa Graber¹

¹*Department of Physics and McGill Space Institute, McGill University, Montreal, Canada*

Correspondence: Department of Physics, McGill University, 3600 rue University, Montreal, QC, H3A 2T8, Canada Email: vanessa.graber@mcgill.ca

Received ; Revised ; Accepted

Although the detailed structure of neutron stars remains unknown, their equilibrium temperatures lie well below the Fermi temperature of dense nuclear matter, suggesting that the nucleons in the stars' core form Cooper pairs and exhibit macroscopic quantum behavior. The presence of such condensates impacts on the neutron stars' large scale properties. Specifically, superconducting protons in the outer core (expected to show type-II properties) alter the stars' magnetism as the magnetic field is no longer locked to the charged plasma but instead confined to fluxtubes. The motion of these structures governs the dynamics of the core magnetic field. To examine if field evolution could be driven on observable timescales, several mechanisms affecting the fluxtube distribution are addressed and characteristic timescales for realistic equations of state estimated. The results suggest that the corresponding timescales are not constant but vary for different densities inside the star, generally being shortest close to the crust-core interface.

Keywords: stars: neutron, stars: magnetic fields, pulsars: general, magnetohydrodynamics (MHD), equation of state

1 INTRODUCTION

Neutron stars host some of the strongest magnetic fields in the Universe. Field strengths (inferred from the stars' dipole spin-down) reach up to 10^{15} G for slowly rotating magnetars, whereas typical radio pulsars have $10^{10} - 10^{13}$ G and recycled millisecond pulsars exhibit $10^8 - 10^{10}$ G. Such fields are expected to strongly influence the dynamics and could provide a natural explanation for various observational features.

Long-term field evolution could, for example, be responsible for field changes in regular pulsars (observed to occur on the order of 10^7 yr (Lyne, Manchester, & Taylor, 1985; Narayan & Ostriker, 1990)), while magnetic field decay on a timescale of about 10^4 yr is generally considered as the driving force behind the high activity of magnetars (Thompson & Duncan, 1995). Additionally, an evolving magnetic field could connect the different classes of neutron stars and provide evolutionary links between them (Harding, 2013; Kaspi, 2010). Despite

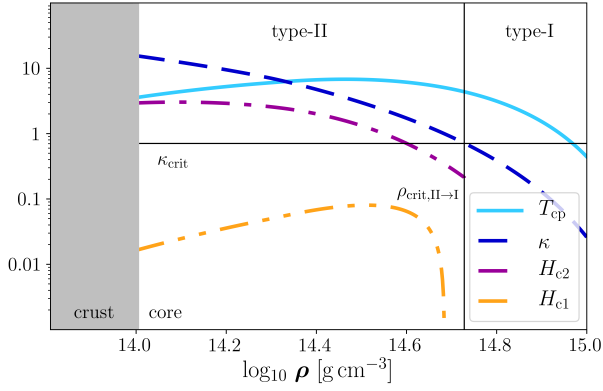


FIGURE 1 Parameters of neutron star superconductivity. Shown are T_{cp} (cyan, solid) (normalized to 10^9 K), κ (blue, dashed) and H_{c2} (purple, dot-dashed) and H_{c1} (yellow, dot-dot-dashed) (normalized to 10^{16} G). The horizontal and vertical line mark κ_{crit} and $\rho_{\text{crit,II}\rightarrow\text{I}}$. The cross-section is given for the NRAPR effective EoS (Steiner et al., 2005) and the energy gap parametrization of Ho et al. (2012).

this, field evolution processes are poorly understood. It also remains unclear if the core, which retains a large fraction of the star’s magnetic energy but is often ignored in theoretical studies (Gourgoulatos & Cumming, 2014; Pons & Geppert, 2007; Viganò et al., 2013), sources the currents that generate the magnetic field and thus takes part in the evolution. If this is indeed the case, there are indications that the core’s high conductivity essentially brings field evolution to a halt (Elfriz, Pons, Rea, Glampedakis, & Viganò, 2016; Graber, Andersson, Glampedakis, & Lander, 2015), leaving the question of how one can reconcile observed magnetic field changes with the theoretical models.

2 TYPE-II SUPERCONDUCTIVITY

Equilibrium neutron stars have $10^6 - 10^8$ K, while the nucleon Fermi temperature is $T_{\text{F}} \sim 10^{12}$ K, implying that these objects are cold enough to contain superfluid neutrons and superconducting protons. The formation of such quantum condensates can be understood within the standard theory of laboratory

superconductors (Bardeen, Cooper, & Schrieffer, 1957). More precisely, the fermions form Cooper pairs due to an attractive contribution to the nucleon-nucleon interaction and detailed calculations give proton transition temperatures in the range of $T_{\text{cp}} \sim 10^9 - 10^{10}$ K (Ho et al., 2012). The type of superconductivity depends on the characteristic length-scales involved. Estimating the Ginzburg-Landau parameter (the ratio of the penetration depth λ and the coherence length ξ_{ft}) leads to

$$\kappa = \frac{\lambda}{\xi_{\text{ft}}} \approx 3.3 \left(\frac{m_{\text{p}}^*}{m} \right)^{3/2} \rho_{14}^{-5/6} \left(\frac{x_{\text{p}}}{0.05} \right)^{-5/6} \left(\frac{T_{\text{cp}}}{10^9 \text{ K}} \right). \quad (1)$$

This is larger than the critical value $\kappa_{\text{crit}} \equiv 1/\sqrt{2}$ and suggests that the neutron star interior is in a type-II state. Here m denotes the baryon mass, $\rho_{14} \equiv \rho/(10^{14} \text{ g cm}^{-3})$ the normalized total mass density and x_{p} the proton fraction. Moreover, m_{p}^* is the proton effective mass, differing from the bare mass m due to entrainment, a non-dissipative interaction present in strongly coupled Fermi systems (Andreev & Bashkin, 1975). The corresponding critical fields read

$$H_{c1} = \frac{\phi_0}{4\pi\lambda^2} \ln\kappa \approx 1.9 \times 10^{14} \left(\frac{m}{m_{\text{p}}^*} \right) \rho_{14} \left(\frac{x_{\text{p}}}{0.05} \right) \text{ G}, \quad (2)$$

$$H_{c2} = \frac{\phi_0}{2\pi\xi_{\text{ft}}^2} \approx 2.1 \times 10^{15} \left(\frac{m_{\text{p}}^*}{m} \right)^2 \rho_{14}^{-2/3} \times \left(\frac{x_{\text{p}}}{0.05} \right)^{-2/3} \left(\frac{T_{\text{cp}}}{10^9 \text{ K}} \right)^2 \text{ G}, \quad (3)$$

where $\ln\kappa \simeq 2$ (Tinkham, 2004) is used to estimate H_{c1} . The density-dependent behavior of these parameters is illustrated in Fig. 1 for the NRAPR effective equation of state (Steiner et al., 2005). Note that most pulsars have $B \lesssim H_{c1}$ and would in principle want to expel magnetic flux from their interior. However as argued in the seminal paper of Baym, Pethick, &

Pines (1969), the conductivity of normal matter is so large that the superconducting transition has to occur at constant flux, implying that the outer core is in a meta-stable type-II state and penetrated by fluxtubes. Fig. 1 further shows that at some density $\rho_{\text{crit,II}\rightarrow\text{I}}$, κ falls below κ_{crit} and an intermediate type-I state is present. As these macroscopic regions of zero and non-zero magnetic flux would be irregularly distributed, it is not obvious how to model such systems theoretically. We thus focus on the outer type-II region, where quantized fluxtubes are arranged in a hexagonal array. Since each fluxtube carries a unit of flux, $\phi_0 \approx 2 \times 10^{-7} \text{ G cm}^2$, the macroscopic magnetic induction B in the star's core is simply obtained by summing all individual flux quanta. This allows one to relate B to the fluxtube surface density and inter-fluxtube distance:

$$\mathcal{N}_{\text{ft}} = \frac{B}{\phi_0} \approx 4.8 \times 10^{18} B_{12} \text{ cm}^{-2}, \quad (4)$$

$$d_{\text{ft}} \simeq \mathcal{N}_{\text{ft}}^{-1/2} \approx 4.6 \times 10^{-10} B_{12}^{-1/2} \text{ cm}, \quad (5)$$

where $B_{12} \equiv B/(10^{12} \text{ G})$. This shows that core field evolution is closely linked to the distribution of fluxtubes and mechanisms driving these structures out of the core towards the crust (where flux subsequently decays) could provide the means to decrease the field strength in the interior. Several effects that influence the fluxtube behavior are analyzed in the following and studied for realistic equations of state (EoSs).

3 FLUXTUBE COUPLING MECHANISMS

3.1 Resistive drag

Electrons can scatter off the fluxtubes' magnetic field (Alpar, Langer, & Sauls, 1984), often referred to as mutual friction in analogy with superfluid hydrodynamics. On mesoscopic

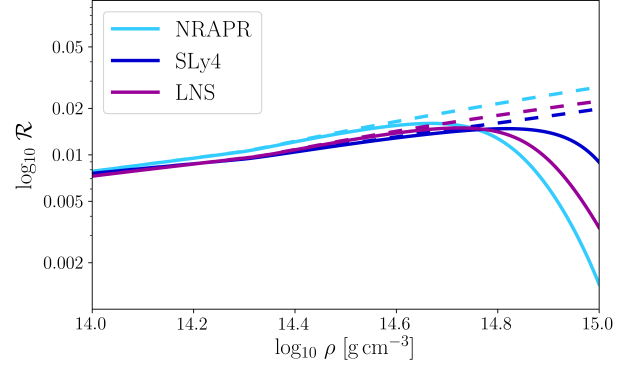


FIGURE 2 Behavior of the resistive drag coefficient as a function of density calculated for three different EoSs and singlet proton pairing. The dashed lines correspond to an approximate solution often found in the literature, which is independent of the energy gap and given by $\mathcal{R} \approx 3\pi^2/(64\lambda k_{\text{Fe}}) \approx 7.9 \times 10^{-3} (m/m_p^*)^{1/2} \rho_{14}^{1/6} (x_p/0.05)^{1/6}$.

scales this drag is proportional to the relative velocity of both components and fully determined by a coefficient \mathcal{R} ; giving $\mathbf{f}_d = \rho_p \kappa \mathcal{R} (\mathbf{v}_e - \mathbf{v}_{\text{ft}})$. Here ρ_p is the proton mass density and $\kappa \approx 2.0 \times 10^{-3} \text{ cm}^2 \text{ s}^{-1}$ the quantum of circulation. Using the formalism of Sauls, Stein, & Serene (1982) \mathcal{R} is found to be

$$\mathcal{R} = \frac{1}{\mathcal{N}_{\text{ft}} \kappa} \frac{E_{\text{Fe}}}{mc^2} \frac{1}{\tau} \approx 1.6 \times 10^{-2} B_{12}^{-1} \left(\frac{k_{\text{Fe}}}{0.75 \text{ fm}^{-1}} \right) \left(\frac{10^{-15} \text{ s}}{\tau} \right), \quad (6)$$

where k_{Fe} denotes the Fermi wave number and τ the velocity relaxation timescale of the electrons. Given an EoS and superconducting gap, τ and \mathcal{R} can be calculated as a function of the star's density. Results for three different parametrized EoSs, namely NRAPR, SLy4 and LNS (see Chamel (2008) for details), together with the proton gap parametrization of Ho et al. (2012) are shown in Fig 2. In the outer core region, the three EoSs do not differ significantly. Note that it has been shown in Graber et al. (2015) by deriving an induction equation for type-II superconducting matter that this resistive drag on its own is too weak to result in field decay on short timescales.

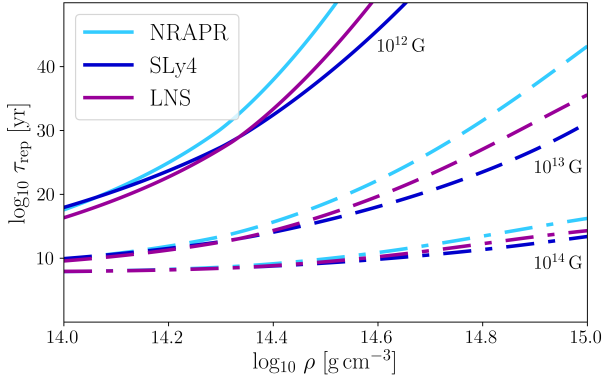


FIGURE 3 Density-dependence of the diffusion timescale estimated from balancing the resistive and the repulsive force. Results are given for three EoSs, three initial field strengths and $L = 10^6$ cm.

3.2 Repulsive interaction

The fluxtubes can also be affected by a repulsive interaction between individual lines. Ignoring their detailed structure, one can determine the interaction energy \mathcal{E}_{int} of two parallel fluxtubes separated by a distance r_{21} and subsequently obtain the standard result for the repulsive force acting on a unit length of fluxtube 1 due to the presence of fluxtube 2 (Tinkham, 2004)

$$\mathbf{f}_{\text{rep}} = -\nabla \mathcal{E}_{\text{int}} = -\frac{\phi_0^2}{8\pi^2 \lambda^3} K_1 \left(\frac{r_{21}}{\lambda} \right) \hat{\mathbf{r}}_{21}. \quad (7)$$

Here, K_1 is a modified Bessel function of second kind and $\hat{\mathbf{r}}_{21}$ the unit vector pointing from fluxtube 1 to 2. To generalize this repulsion to a fluxtube lattice, individual contributions simply have to be summed up. For a perfectly hexagonal array, the net force on each line would exactly vanish and no field changes take place. However, due to the large number of fluxtubes it is likely that some irregularity affects the type-II state in neutron stars; in analogy with laboratory systems we would specifically expect the long-range order of the lattice to be destroyed. This would cause a gradient in the fluxtube density, directly related to a non-zero net force on the fluxtubes and would

thus drive field evolution. In an averaged picture, the resulting force should be of the form $\mathbf{f}_{\text{rep}} = -g(\mathcal{N}_{\text{ft}}) \nabla \mathcal{N}_{\text{ft}}$. For pulsars with $B \lesssim 10^{14}$ G the calculation of $g(\mathcal{N}_{\text{ft}})$ simplifies due to the hierarchy of the relevant length-scales. Since $d_{\text{ft}} \simeq r_{21} \gtrsim \lambda$, K_1 can be approximated as a decaying exponential and the summation reduced to the six nearest neighbors. Looking at the detailed geometry, one arrives at ¹

$$g(\mathcal{N}_{\text{ft}}) \simeq \frac{3\phi_0^2}{32\sqrt{2}\pi^{3/2}} \left(\frac{\sqrt{2}\mathcal{N}_{\text{ft}}^{-1/2}}{3^{1/4}\lambda} \right)^{7/2} e^{-\frac{\sqrt{2}\mathcal{N}_{\text{ft}}^{-1/2}}{3^{1/4}\lambda}}. \quad (8)$$

We now consider a simple scenario, where the resistive and repulsive mechanisms affect the type-II state. Neglecting fluxtube inertia, the force balance in this steady state reads $\sum \mathbf{f} = -g(\mathcal{N}_{\text{ft}}) \nabla \mathcal{N}_{\text{ft}} - \rho_p \kappa \mathcal{R} \mathbf{v}_{\text{ft}} = 0$. Solving this for \mathbf{v}_{ft} , the resulting expression can be combined with the continuity equation for \mathcal{N}_{ft} (see Glampedakis, Andersson, & Samuelsson (2011) for details) to obtain a non-linear diffusion equation for the evolution of the fluxtubes, i.e. the magnetic induction:

$$0 = \partial_t \mathcal{N}_{\text{ft}} - \nabla \cdot \left(\frac{\mathcal{N}_{\text{ft}} g(\mathcal{N}_{\text{ft}})}{\rho_p \kappa \mathcal{R}} \nabla \mathcal{N}_{\text{ft}} \right). \quad (9)$$

Instead of solving this equation, we simply extract a diffusion timescale. For a characteristic length-scale L , one has

$$\tau_{\text{rep}} = \frac{L^2 \rho_p \kappa \mathcal{R}}{\mathcal{N}_{\text{ft}} g(\mathcal{N}_{\text{ft}})}. \quad (10)$$

Estimates for different EoSs, $L = 10^6$ cm and three initial magnetic inductions are illustrated in Fig. 3, showing strong

¹ We note that the expression (8) does not agree with the equivalent result given by Kocharovskiy, Kocharovskiy, & Kukushkin (1996). We further point out that Istomin & Semerikov (2016) who study field evolution in accreting neutron stars are likely overestimating the effect of the repulsive force due to an erroneous approximation of \mathbf{f}_{rep} in the limit $d_{\text{ft}} \ll \lambda$.

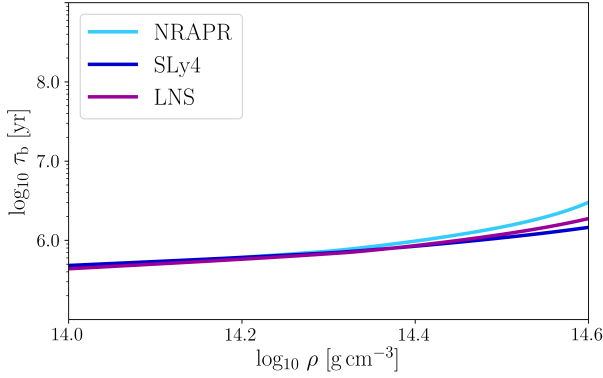


FIGURE 4 Density-dependence of the diffusion timescale estimated from balancing the resistive and the buoyancy force. Results are given for three EoSs, three initial fields and $L = 10^6$ cm.

variability with density. For all field strengths, τ_{rep} is smallest at low densities and increases significantly towards higher densities as a result of the exponential in Eqn. (8). For standard pulsars, τ_{rep} exceeds the age of the Universe and no field evolution takes place, but it decreases for higher fields and reaches $\sim 10^7$ yr for 10^{14} G. Taking into account that this estimate sensitively depends on L , which could also take values of 10^5 cm (Lander, 2014), Eqn. (9) could potentially capture field evolution in magnetars. Note that Eqn. (8) is however not suitable to model fields $B \gtrsim 10^{14}$ G, since then $r_{21} \lesssim \lambda$ and the assumptions in deriving $g(\mathcal{N}_{\text{ft}})$ are no longer valid. Studying this regime will be left for future work. One final note of caution: the repulsive force does not necessarily have to expel the field out of the star’s core, i.e. lead to field decay. Instead this mechanism results in fluxtube motion in the direction opposite to the density gradient $\nabla \mathcal{N}_{\text{ft}}$ and thus strongly depends on the (unknown) details of the magnetic field configuration.

3.3 Buoyancy

Fluxtubes are buoyant structures as a result of the magnetic pressure inside their cores. This creates a radially acting lift force, f_b , trying to drive the fluxtubes out of the core (Harvey,

Ruderman, & Shaham, 1986; Muslimov & Tsygan, 1985).²

The buoyancy force can be related to the gradient of the superconducting magnetic pressure, which in the limit $B \lesssim H_{c1}$ satisfied by the neutron star is given by $P = H_{c1} B / 4\pi$ (Easson & Pethick, 1977). Per unit length of fluxtube, one finds

$$f_b = \frac{|-\nabla P|}{\mathcal{N}_{\text{ft}}} \simeq \frac{H_{c1} B}{\mathcal{N}_{\text{ft}} 4\pi L} = \frac{H_{c1} \phi_0}{4\pi L}. \quad (11)$$

Balancing the resistive drag with the buoyancy force, one can arrive at an analogous non-linear diffusion equation as for the repulsive interaction. The respective timescale now reads

$$\tau_b = L^2 \rho_p \kappa \mathcal{R} \frac{16\pi^2 \lambda^2}{\phi_0^2 \ln \kappa}. \quad (12)$$

Estimates for $L = 10^6$ cm and three EoSs are given in Fig. 4. This shows that τ_b is shortest close to the crust-core interface with a minimum of $\sim 10^5$ yr and increases by about one order of magnitude towards the inner core. These timescales are of the order of observed field changes and buoyancy could potentially explain the physics behind the field evolution. However note that recent self-consistent magneto-thermal simulations of superconducting cores by Elfritz et al. (2016) indicate that buoyancy is too weak to drive observable field evolution.

4 DISCUSSION AND CONCLUSIONS

We have studied various mechanisms expected to affect superconducting fluxtubes in the outer neutron star core and calculated characteristic timescales for these processes. Using three realistic EoSs these timescales were estimated for the cross-section of a neutron star and the resulting magnetic field

² See also Dommes & Gusakov (2017) for a discussion of the buoyancy force in a two-component system.

changes were found to act on shortest timescales at low densities, close to the crust-core interface. While our simple estimates suggest that repulsive interaction and buoyancy might be able to drive field evolution on observable timescales, it is difficult to translate this to realistic systems since more work is needed to account for additional physics that likely affect the neutron star's magnetism. This specifically involves the question of how fluxtubes interact with neutron vortices that result from the quantization of the neutron superfluid's rotation in the outer core. Further, it remains unclear if the outer core is indeed in a pure type-II or a mixed type-II/type-I state (Alford & Good, 2008; Charbonneau & Zhitnitsky, 2007; Link, 2003). The presence of such a regime where macroscopic flux-free regions alternate with type-II domains should strongly depend on the star's initial magnetic flux distribution and the microphysics of the superconducting phase transition. Exploring the analogy with laboratory condensates could be beneficial in answering this questions (Grabber, Andersson, & Hogg, 2017).

Acknowledgments

VG is supported by a McGill Space Institute postdoc fellowship and the Trottier Chair in Astrophysics and Cosmology.

References

Alford, M., & Good, G. 2008, *Phys. Rev. B*, 78(2), 024510.

Alpar, M. A., Langer, S., & Sauls, J. 1984, *ApJ*, 282, 533.

Andreev, A., & Bashkin, E. 1975, *Sov. Phys. JETP*, 42(1), 164.

Bardeen, J., Cooper, L., & Schrieffer, J. 1957, *Phys. Rev.*, 108(5), 1175.

Baym, G., Pethick, C., & Pines, D. 1969, *Nature*, 224(5220), 673.

Chamel, N. 2008, *MNRAS*, 388(2), 737.

Charbonneau, J., & Zhitnitsky, A. 2007, *Phys. Rev. C*, 76(1),

015801.

Dommes, V., & Gusakov, M. 2017, *MNRAS*, 467(1), L115.

Easson, I., & Pethick, C. 1977, *Phys. Rev. D*, 16(2), 275.

Elfritz, J., Pons, J., Rea, N., Glampedakis, K., & Viganò, D. 2016, *MNRAS*, 456(4), 4461.

Glampedakis, K., Andersson, N., & Samuelsson, L. 2011, *MNRAS*, 410(2), 805.

Gourgouliatos, K., & Cumming, A. 2014, *MNRAS*, 438(2), 1618.

Grabber, V., Andersson, N., Glampedakis, K., & Lander, S. 2015, *MNRAS*, 453(1), 671.

Grabber, V., Andersson, N., & Hogg, M. 2017, *Int. J. Mod. Phys. D*, 1730015.

Harding, A. 2013, *Front. Phys.*, 8(6), 679.

Harvey, J., Ruderman, M., & Shaham, J. 1986, *Phys. Rev. D*, 33(8), 2084.

Ho, W., Glampedakis, K., & Andersson, N. 2012, *MNRAS*, 422(3), 2632.

Istomin, Y., & Semerikov, I. 2016, *MNRAS*, 455(2), 1938.

Kaspi, V. 2010, *Proc. Natl. Acad. Sci.*, 107(16), 7147.

Kocharovskiy, V., Kocharovskiy, V., & Kukushkin, V. 1996, *Radio-physics and Quantum Electronics*, 39(1), 18.

Lander, S. 2014, *MNRAS*, 437(1), 424.

Link, B. 2003, *Phys. Rev. Lett.*, 91(10), 101101.

Lyne, A., Manchester, R., & Taylor, J. 1985, *MNRAS*, 213(3), 613.

Muslimov, A. G., & Tsygan, A. I. 1985, *Sov. Astron. Lett.*, 11, 80.

Narayan, R., & Ostriker, J. 1990, *ApJ*, 352, 222.

Pons, J. A., & Geppert, U. 2007, *A&A*, 470(1), 303.

Sauls, J., Stein, D., & Serene, J. 1982, *Phys. Rev. D*, 25(4), 967.

Steiner, A., Prakash, M., Lattimer, J., & Ellis, P. 2005, *Phys. Rep.*, 411(6), 325.

Thompson, C., & Duncan, R. 1995, *MNRAS*, 275(2), 255.

Tinkham, M. 2004, *Introduction to Superconductivity* (2nd ed.), New York: Dover Press.

Viganò, D., Rea, N., Pons, J., Perna, R., Aguilera, D., & Miralles, J. 2013, *MNRAS*, 434(1), 123.

